JOURNAL OF Materials CHEMISTRY

New $n=2$ members of the $Li_2Sr_{n-1}M_nO_{3n+1}$ family, closely related to the Ruddlesden–Popper phases: structure and non-stoichiometry

N. Floros, C. Michel,* M. Hervieu and B. Raveau

Laboratoire CRISMAT, UMR 6508 associée au CNRS, ISMRA et Université de Caen, 6, Boulevard du Maréchal Juin, 14050 CAEN Cedex, France. E-mail: Claude MICHEL, claude.michel@ismra.fr

Received 2nd June 1999, Accepted 17th September 1999

New $n=2$ members of the $Li_2Sr_{n-1}M_nO_{3n+1}$ series closely related to the RP phases have been synthesized by solid state reaction for the first time: $Li_2SrNb_2O_7$, $Li_2SrTa_2O_7$, $Li_2EuTa_2O_7$. The detailed structure determination of $Li_2SrNb_2O_7$ performed by neutron diffraction and electron microscopy shows that it crystallizes in the space group *Cmcm* [$a=18.0071(5)$, $b=5.5979(3)$, $c=5.5920(3)$ Å], *i.e.* with a symmetry different from that of $LiAM_2O_7$ and $Li_2AM_2O_7$ previously synthesized by chemical or electrochemical intercalation. The double perovskite layers [$SrNb_2O_6$] are puckered due to a tilting of their [001] octahedral rows alternately in opposite directions while the tetrahedral [Li_2O] layers are significantly distorted. The possibility of cationic non-stoichiometry in both Li and Sr sites is demonstrated by the synthesis of $Li_2Sr_{1-x}Ln_{2x/3}Nb_2O_7$ (Ln = La, Nd) and $Li_{2-x}Sr_{1-x}La_xNb_2O_7$ oxides. The stability of these phases is discussed in terms of matching of the octahedral and tetrahedral layers, taking into consideration the tilting of the octahedra, itself influenced by the size of the A site cations and the cationic non-stoichiometry. An extension to $n=3$ members is made, with the synthesis of the oxides $Li_2Sr_{1.5}Nb_3O_{10}$ and $Li_2Ca_{1.5}Nb_3O_{10}$.

Introduction

The strontium-rich titanates discovered more than forty years ago by Ruddlesden and Popper[1] have been the starting point of numerous investigations into the generation of new structural types and new properties. These 'RP' phases with the generic formulation $A_{n+1}M_nO_{3n+1}$ are generally described as intergrowths of multiple perovskite layers $A_nM_nO_{3n}$ with single rock salt layers AO, A being a divalent or trivalent cation with a large size and M being one or several transition elements. Using ion exchange reaction methods, a second series of closely related structures $A'A_{n-1}M_nO_{3n+1}$ were generated for A′ = Li, Na, Ag, Co, Cu, Zn; A = La, Ca and M = Nb, Ti.[2–6] These cation deficient oxides exhibit a geometry and a relative position of the multiple perovskite layers similar to those of the RP phases. Two successive perovskite layers are brought closer together, so that tetrahedral sites are formed, which are half occupied by A′ cations, forming A′O tetrahedral layers instead of AO rock salt layers. As a consequence, the A cations sitting at the boundary of the octahedral and of these tetrahedral layers are removed forming $A_{n-1}M_nO_{3n}$ layers instead of $A_nM_nO_{3n}$ layers. This structural analysis suggests that it should be possible to synthesize a series of isostructural oxides with a larger A′ content, with the formula $A'_2A_{n-1}M_nO_{3n+1}$, corresponding to complete occupation of the tetrahedral sites. The synthesis of the $n=2$ members $Li_2LaNb_2O_7$ and $Li_2LaTa_2O_7$ and $n=3$ member $Li_2La_2Ta_3O_{10}$ by chemical and electrochemical intercalation of lithium[7–9] supports this viewpoint. Nevertheless, only one member of this series $Li_2Sr_{1.5}Nb_3O_{10}$ has been synthesized, as yet, by solid state reaction, by Bhuvanesh *et al.*[10] This $n=3$ member is moreover of interest for its strontium deficiency and for its structural complexity.

Here, we have investigated the crystal chemistry of the $n=2$ members of the $Li_2A_{n-1}M_nO_{3n+1}$ family. Several $n=2$ members, $Li_2Sr_{1-x}La_{2x/3}Nb_2O_7$ ($0\leqslant x\leqslant 0.90$) and $Li_2Sr_{1-x}Nd_{2x/3}Nb_2O_7$ ($0\leqslant x\leqslant 0.50$), as well as $Li_2SrTa_2O_7$ and $Li_2Sr_{1-x}Eu_xTa_2O_7$ have been synthesized for the first time, using solid state reactions. Detailed neutron diffraction and electron microscopy study of $Li_2SrNb_2O_7$ shows that the structure of this phase differs from that obtained for $Li_2LaM_2O_7$[7,9] by its symmetry, involving a cooperative tilting of the octahedra leading to distorted LiO_4 tetrahedra.

Experimental

The phases $Li_2Sr_{1-x}Ln_{2x/3}Nb_2O_7$ (Ln = La, Nd) and $Li_2SrTa_2O_7$ were synthesized in air in two steps. Intimate mixtures of Li_2CO_3, $SrCO_3$, Nb_2O_5 or Ta_2O_5, (and Ln_2O_3 where required) in stoichiometric proportions were heated in an alumina crucible at 600 °C for 12 h. Then they were ground again, pressed into bars and heated at 1100 °C for 6 h in an alumina crucible. The compounds $Li_2Sr_{1-x}Eu_xTa_2O_7$ were also prepared in two steps but in a different manner in order to avoid the oxidization of Eu(II) into Eu(III). The first step was also carried out in air at 600 °C but with different proportions of Li_2CO_3, $SrCO_3$, Eu_2O_3 and Ta_2O_5 according to the formula $Li_2Sr_{1-x}Eu_xTa_{2-0.2x}O_7$. After decarbonation, the products were added in a second step with $0.2x$ metallic tantalum, pressed into bars and heated at 1100 °C for 12 h in an evacuated silica tube, containing zirconium turnings in order to avoid possible oxidation.

Lithium and strontium were analyzed using a Varian Atomic Absorption Spectrometer SpectrAA-20 with air–acetylene flame (lithium) or nitrous oxide–acetylene flame (strontium) for some samples to verify a possible loss of lithium during synthesis.

Lattice constants were refined from X-ray powder data on a Philips vertical diffractometer equipped with a secondary graphite monochromator and working with Cu-Kα radiation. Data were collected by step scanning of 0.03° in the range 2θ 8–120°. Neutron diffraction data were collected at room temperature at the LLB (Saclay, France) on the 3T2 diffactometer using a wavelength $\lambda=1.2251$ Å. The diffraction pattern was recorded over the angular range $9\leqslant 2\theta\leqslant 125.7°$ in 0.05° (2θ) increments and treated by profile analysis with the FULLPROF program (version 3.5-LLB-JRC).[11]

The electron diffraction (ED) study was carried out using a JEOL 200 CX microscope fitted with an eucentric goniometer ($\pm 60^\circ$) and high resolution electron microscopy (HREM) images were obtained with a TOPCON 02B microscope operating at 200 kV and having a point resolution of 1.8 Å. HREM image calculations were carried out with the Mac-Tempas multislice program. Both microscopes were equipped with an energy dispersive spectroscopy (EDS) analyser.

Magnetic measurements were carried out using a Quantum Design SQUID magnetometer, between 5 and 400 K, in a magnetic field of 3000 G.

Results and discussion

$Li_2SrNb_2O_7$: electron microscopy and neutron diffraction study

For the above synthesis conditions, a pure phase is obtained for the nominal composition $Li_2SrNb_2O_7$. Chemical analysis using cationic absorption spectroscopy indicates a small lithium deficiency, indicating departure of Li_2O during the synthesis. Nevertheless the Li deficiency is very low, not exceeding 4% of the theoretical value.

The electron diffraction (ED) investigation, coupled with EDS analysis performed on more than 50 microcrystals shows the substantial homogeneity of the sample, the Sr/Nb ratio remaining close to the nominal value at the limit of the experimental error. Examination of the ED patterns (Fig. 1) shows a system of intense reflections characteristic of the classical tetragonal cell '$3.9 \times 3.9 \times 18$ Å' with space group $I4/mmm$, where 3.9 Å corresponds to the a_p parameter of the cubic perovskite subcell. However the reconstruction of reciprocal space, carried out by tilting around the crystallographic axes, indicates the presence of weak extra reflections, leading to an actual orthorhombic cell, with $a \cong 18$ Å and $b \approx c \cong a_p\sqrt{2} \approx 5.6$ Å. The corresponding reflection conditions, hkl, $h+k=2n$ and $h0l$, h, $l=2n$, are compatible with the space groups $Cmcm$, $C2cm$ and $Cmc2_1$.

The interpretation of the ED patterns is complicated by the existence of three types of phenomena:

(i) twinning phenomena are systematically observed in the crystallites; this is illustrated in Fig. 2(a) with the superposition of $[0\bar{1}2]$ and $[0\bar{2}1]$ patterns. This twinning results from the loss of tetragonal symmetry.

(ii) In the [100] patterns, the 011 reflections are sometimes observed but are always very weak. These extra reflections can be generated by two types of artefacts: first, double diffraction phenomena as soon as [001] and [010] areas coexist and second, the existence of streaks along a^*, as further discussed below. However, the different ED analyses suggest that locally, the reflection conditions are violated, involving a lowering of the symmetry.

(iii) Very weak diffuse streaks are sometimes observed along a^*. One example of a particularly streaky direction is enlarged in Fig. 2(b). These streaks are generated by the existence of stacking defects along $\vec{a}$ as will be shown from the high resolution electron microscopy study.

In contrast to the X-ray powder diffraction pattern [Fig. 3(a)] which can be indexed in a tetragonal cell '$a_p \times a_p \times c$', the neutron powder diffraction pattern shows numerous weak extra peaks [Fig. 3(b)] indicative of the supercell '$a_p\sqrt{2} \times a_p\sqrt{2} \times c$'. The use of the $Cmcm$ space group implies a rotation of axes with regard to the above notation, '$a \times a_p\sqrt{2} \times a_p\sqrt{2}$', and the pattern was then indexed in an orthorhombic cell with $a=18.0071(5)$, $b=5.5979(3)$ and $c=5.5920(3)$ Å. The comparison between XRPD and NPD data clearly suggests that the orthorhombic symmetry mainly originates from the oxygen contribution. Thus structure calculations were performed from NPD data in the $Cmcm$ space group (Table 1). For Sr, Nb, O(1) and O(2) atoms, the starting y value was deduced from corresponding positions in the $I4/mmm$ space group, *i.e.* $y=1/4$ or 3/4.

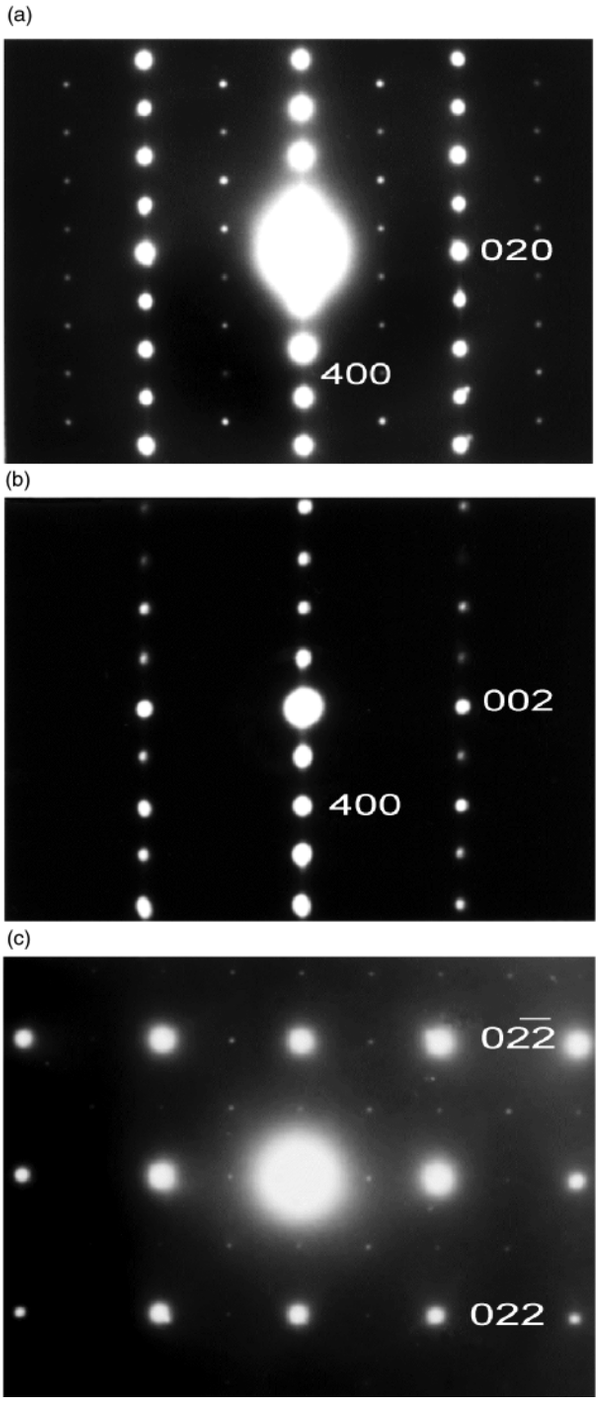

Fig. 1 ED patterns of $Li_2SrNb_2O_7$: (a) [001], (b) [010], (c) [100] (note that oriented domains and double diffraction generate the apparent existence of every $0kl$ reflection).

The refinements of the other variable atomic parameters and isotropic thermal parameters allowed the profile and Bragg R factors to converge to $R_p=11.8\%$ and $R_B=12.7\%$, the B values of the oxygen atoms located at the Sr level remaining rather high, *i.e.* close to 3 Å^2. Fourier difference maps sections calculated at the level of all oxygen atoms showed without ambiguity that O(1) and O(2) were displaced along $\vec{b}$ from their 'ideal' $y=3/4$ position, whereas O(3) and O(4) were displaced along $\vec{a}$. Thus the x values of O(3) and O(4) and the y values of O(1) and O(2) were refined in a second step, and all the variables were then refined in a third step. A substantial decrease in the residuals was obtained: $R_p=8.1\%$, $R_B=6.7\%$.

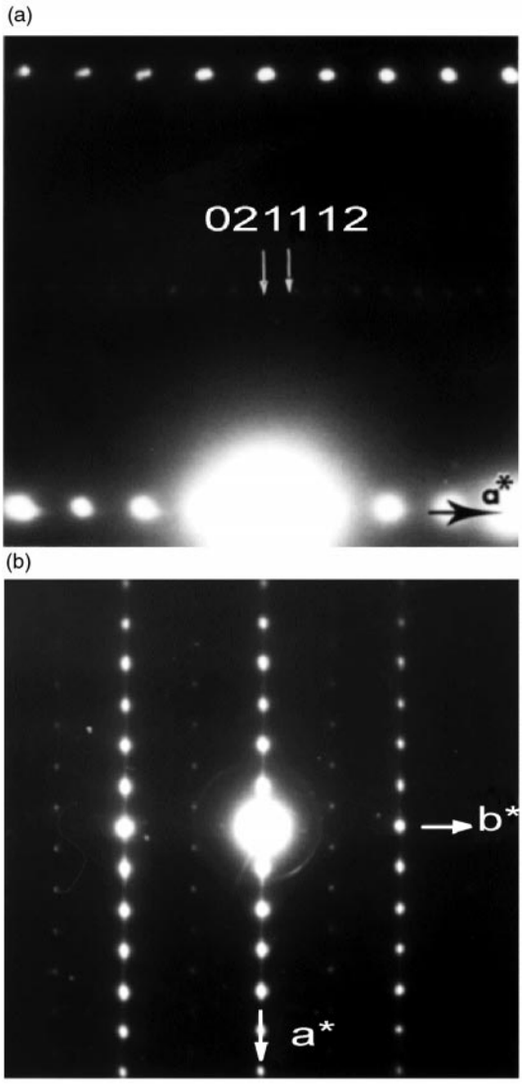

Fig. 2 (a) Enlarged $[0\bar{1}2]$ and $[0\bar{2}1]$ ED patterns of $Li_2SrNb_2O_7$ which are systematically superposed owing to twinning phenomena. (b) Streaks along $\vec{a}^*$ are generated by intergrowth defects.

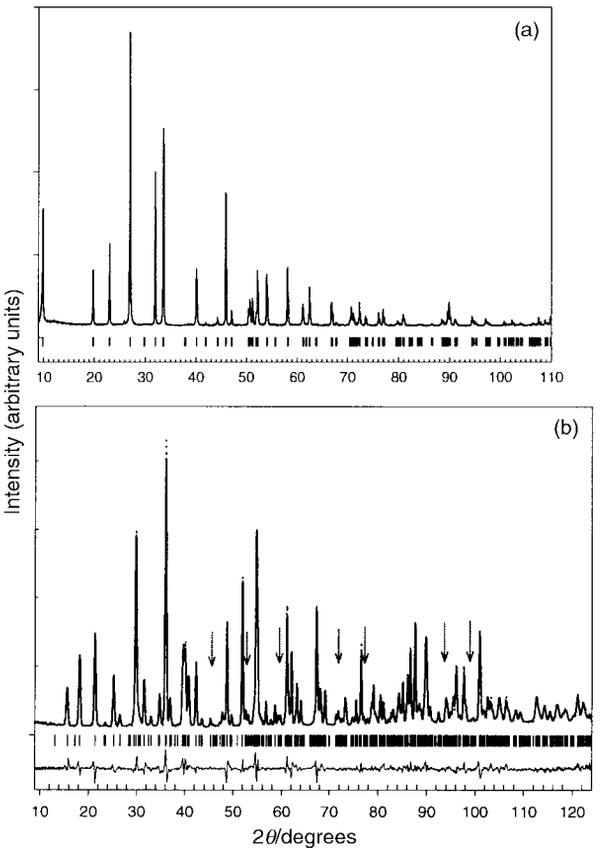

Fig. 3 (a) Powder X-ray diffraction pattern of $Li_2SrNb_2O_7$. The vertical bars are the Bragg positions of the reflections in the space group *I*4/*mmm*. The weak diffraction peak at $2\theta = 25.7^\circ$ cannot be indexed using a C space group. (b) Experimental (dotted line) calculated and difference (solid lines) powder neutron diffraction patterns of $Li_2SrNb_2O_7$ after structural refinements in the space group *Cmcm*. Vertical arrows indicate the reflections which cannot be indexed in the *I*4/*mmm* space group.

At this stage, a comparison between experimental and calculated intensities showed that for *h*00 reflections the observed intensity was systematically slightly higher than the calculated value. This suggested a preferential orientation along [100] as observed by X-ray diffraction techniques. Taking into account this phenomenon, refinement of all variables lowered the residuals to $R_p = 6.2\%$, $R_{wp} = 8.0\%$, $R_B = 4.8\%$ for the atomic parameters listed in Table 1.

This structural study shows that $Li_2SrNb_2O_7$ exhibits, similarly to other niobates and tantalates $Li_2LaM_2O_7$ and $Li_2LaM_2O_7$,[6–9] double perovskite layers $[SrM_2O_6]$ interleaved with tetrahedral layers $[Li_2O]$ (Fig. 4). However, most important, it differs from the latter by its symmetry which implies a puckering of the $[NbO_2]_\infty$ layers owing to the tilting of the [001] rows of NbO_6 octahedra alternately in opposite directions with respect to *a*. As a result, the LiO_4 tetrahedra are strongly distorted with two short and two long Li–O bonds (Table 2), in contrast to other previously described $LiLaM_2O_7$ or $Li_2LaM_2O_7$ oxides.[7,9] These tetrahedra are also flattened and a fifth oxygen neighbour lies at 2.27 Å, so that the lithium coordination may be described as intermediate between distorted tetrahedral and distorted pyramidal. The Sr–O distances (Table 2) are close to those commonly observed in perovskites. The NbO_6 octahedra exhibit four very similar equatorial Nb–O bonds (1.98–2.00 Å), whereas along $\vec{a}$, a short apical Nb–O distance (1.86 Å) alternates with a longer one (2.08 Å) corresponding to Nb–O–Li and Nb–O–Nb bonds, respectively. Such a distortion is quite similar to that encountered in homologous niobates and tantalates. The mean value of the interatomic Nb–O distances, 1.984 Å, is typical for compounds involving Nb(v). The in-plane and out-of-plane interatomic Nb–Nb distances, 3.96 and 4.14 Å, respectively, show that in the perovskite slabs, the perovskite sub-cell is tetragonally distorted.

In order to understand the presence of streaks in the ED patterns, high resolution electron microscopy (HREM) was carried out. The experimental [011] HREM images were compared to the theoretical ones, calculated on the basis of the refined positional parameters (Table 1). One example of a characteristic [100] enlarged image is given in Fig. 5(a) for a focus value of *ca.* −40 nm; the Sr and Nb positions are correlated to the small gray dots whereas the $[O–Li_2–O]$ slices appear as a double row of staggered dark and bright dots. Such images allow easy interpretation of the nature of the atomic layers stacked along *a* and confirm that the stacking mode of the different layers along [100] is that proposed. However, depending on the focus value, important local contrast variations are observed at the level of the Sr rows. This is clearly visible for a focus value close to −55 nm [Fig. 5(b)] where the Sr positions appear as very bright dots : along a Sr row (see, for example, superimposed arrows) the brightness of the corresponding dots does not vary regularly as expected from a simple thickness effect (see, for example, the row parallel to [011] between the two arrows). Such a variation of contrast could be correlated to cation deficiency and/or cation displacement. Since XRPD refinements, which are more

Table 1 Crystal parameters for $Li_2SrNb_2O_7$[a]

Atom	Site	*x*	*y*	*z*	*B*/Å^2
Li	8e	0.2596(5)	0.0	0.0	1.4(1)
Sr	4c	0.0	0.2514(8)	0.25	0.65(3)
Nb	8m	0.1150(1)	0.7503(6)	0.25	0.40(2)
O(1)	4c	0.0	0.7125(8)	0.25	0.53(8)
O(2)	8g	0.2182(1)	0.7766(7)	0.25	0.67(4)
O(3)	8e	0.6144(1)	0.0	0.0	0.78(4)
O(4)	8e	0.0982(1)	0.0	0.0	0.53(4)

[a]Space group *Cmcm*, $a=18.0071(5)$, $b=5.5979(3)$, $c=5.5920(3)$ Å, $R_p=6.2\%$, $R_{wp}=8.0\%$, $R_B=4.8\%$: preferential orientation parameter $G=1.062(2)$.

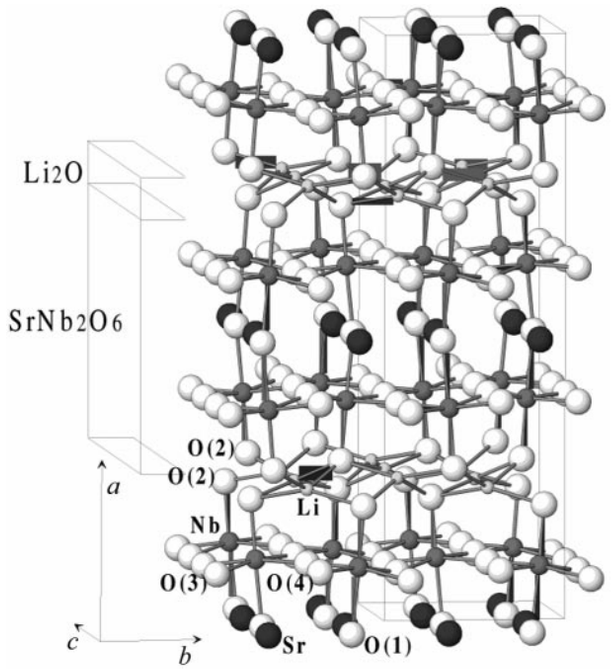

Fig. 4 Perspective drawing of the structure of $Li_2SrNb_2O_7$.

sensitive than NPD for cations, show in agreement with EDS and chemical analyses, that there is no significant deviation of the Sr site occupancy from 100%, the second factor is likely to be responsible for the phenomenon and could be related to the local lowering of symmetry as observed by ED. In this image [Fig. 5(b)], intergrowth defects are also detected. Instead of a single row of bright spots correlated to the Sr positions, one row of gray dots sandwiched between two rows of bright dots is observed. This can be easily interpreted as the insertion of additional layers, one $[SrO]_\infty$ and one $[NbO_2]_\infty$ layer, *i.e.* an additional perovskite slice. This therefore corresponds to the local formation of an $n=3$ member within the $n=2$ matrix.

Synthesis and characterization of other $n=2$ members

$Li_2SrNb_2O_7$ is to date the only $n=2$ member of the $A_{n-1}M_nO_{3n+1}$ series with tetrahedral layers to be synthesized by solid state reaction. In order to understand the stability of such a structure and the cationic non-stoichiometry, various niobates and tantalates with the formula $Li_2A_{1-x}M_2O_7$, were investigated.

Complete substitution of tantalum for niobium is possible. The tantalate $Li_2SrTa_2O_7$ exhibits very similar parameters (Table 3) and its ED study shows clearly that it belongs to the same space group *Cmcm*.

The possibility of replacing strontium by divalent europium was considered. The synthesis of the phase $Li_2EuNb_2O_7$ was unsuccessful in accord with the fact that Eu(II) reduces Nb(V) according to the redox reaction Nb(V)+Eu(II)→Nb(IV)+Eu(III). By contrast, the phase $Li_2Sr_{1-x}Eu_xTa_2O_7$ could be synthesized for $0.80\leqslant x\leqslant 1$, with cell parameters very similar to those of $Li_2SrTa_2O_7$ (Table 3), in accord with the similar size of Eu^{2+} and Sr^{2+}. Variable temperature magnetic susceptibility measurements of these compounds show paramagnetism, with a Curie law behavior in the range 10–340 K (Fig. 6). The fitting of the $\chi^{-1}(T)$ curves leads to an effective magnetic moment of 7.54 μ_B per mol europium, which can be compared with the theoretical values of 7.94 μ_B assuming divalent europium and 3.82 μ_B assuming trivalent europium and tetravalent tantalum. This confirms that the majority of europium is divalent, but nevertheless the possibility of the presence of a small fraction of trivalent europium, according to the formula $Li_2Sr_{1-x}Eu_{x-y}{}^{II}Eu_y{}^{III}Ta_{2-y}{}^{V}Ta_y{}^{IV}O_7$ ($y\leqslant 0.05$) cannot be ruled out.

In order to test the possibility of cation non-stoichiometry in this structure, we have studied the substitution of a trivalent lanthanide for strontium in $Li_2SrNb_2O_7$. The synthesis of $Li_2Sr_{1-x}La_{2x/3}Nb_2O_7$, with a large homogeneity range ($0\leqslant x\leqslant 0.90$) shows that a rather large cation deficiency on the Sr sites (30%) does not alter the stability of the structure. This is in agreement with the results obtained by Bhuvanesh *et al.*[10] who found a comparable non-stoichiometry (20%) in the $n=3$ member $Li_2Sr_{1.5}Nb_3O_{10}$. Nevertheless, as the size of the lanthanide cation decreases, the homogeneity range of the phase decreases, as shown for $Li_2Sr_{1-x}Nd_{2x/3}Nb_2O_7$ for which *x* only ranges from 0 to 0.50. Thus, it seems that the size of the A site cation is a limiting factor for the stability of the $Li_2A_{1-x}Nb_2O_7$ phases. This viewpoint is also supported by the fact that attempts to prepare the homologous phase $Li_2CaNb_2O_7$ by solid state reaction were unsuccessful. This behavior can be explained by the fact that the size of the A site cation may influence significantly the tilting of the NbO_6 octahedra in the double perovskite layers, but that this tilting is, on the other hand, limited by the matching between the octahedral ANb_2O_6 and the tetrahedral Li_2O layers. The evolution of the cell parameters of the oxides $Li_2Sr_{1-x}Ln_{2x/3}$

Table 2 Selected interatomic distances (Å) for $Li_2SrNb_2O_7$

Li–O(2)	2.018(4)	×2	Sr–O(1)	3.016(6)	×1
Li–O(2)	2.124(3)	×2	Sr–O(1)	2.582(6)	×1
Li–O(3)	2.270(9)	×1	Sr–O(1)	2.803(1)	×2
			Sr–O(3)	2.852(3)	×4
Nb–O(1)	2.082(2)	×1	Sr–O(4)	2.652(1)	×4
Nb–O(2)	1.864(3)	×1			
Nb–O(3)	1.979(2)	×2			
Nb–O(4)	2.000(2)	×2			

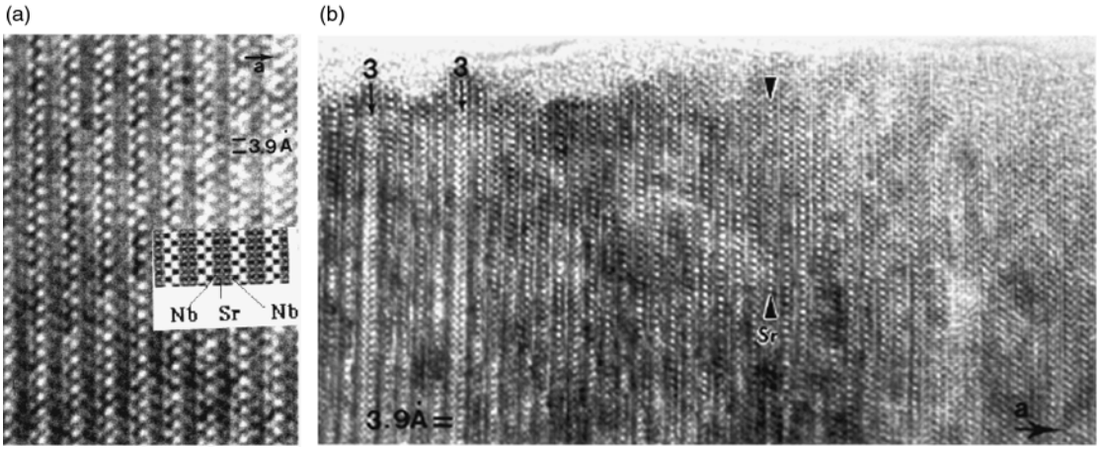

Fig. 5 (a) enlarged [100] HREM image of $Li_2SrNb_2O_7$ for a focus value close to −40 nm which illustrates the layer stacking mode along $\vec{a}$. (b) HREM image showing local contrast variations at the level of the Sr rows and intergrowth defects.

Nb_2O_7 (Table 3) suggests indeed that this tilting of the NbO_6 octahedra is greatly affected by substitution of Sr by Ln. The *b* and *c* parameters decrease as *x* increases for both series, La^{3+} and Nd^{3+}, in accord with the smaller size of these cations compared to Sr^{2+}. By contrast, *a* increases with *x* in both cases up to $x=0.50$, and, then, decreases again in the case of lanthanum for $x>0.50$. These results suggest that the distortion of the perovskite sub-cell (proportional to *a*/*b* or *a*/*c*), and probably the tilting of the octahedra is greatly influenced by the size of the A site cations and by cation deficiency. While analysis using atomic absorption spectroscopy shows that the lithium deficiency is $<4\%$ the possibility of lithium non-stoichiometry in these oxides, according to the formula $Li_{2-x}Sr_{1-x}La_xNb_2O_7$ must be considered. The synthesis of the oxide $Li_{1.8}Sr_{0.8}La_{0.2}Nb_2O_7$ ($x=0.2$) as a single phase following the same process confirms our statement. The cell parameters of this phase (Table 3) show its very different behavior, compared to all other $Li_2Sr_{1-x}La_{2x/3}Nb_2O_7$ oxides. The *a* parameter of $Li_{1.8}Sr_{0.8}La_{0.2}Nb_2O_7$ is significantly larger than for the other oxides. This result is in accord with those previously found for $LiAM_2O_7$ oxides obtained by chemical or electrochemical intercalation.[3,6] These compounds crystallise in tetragonal symmetry (space group *I*4/*mmm*) and exhibit a *c* parameter (*ca.* 20.4 Å) larger than that observed in $Li_2AM_2O_7$ oxides[7,9] (18.5–19 Å). Thus, it is probable that the distortion of the perovskite sub-cell and consequently the tilting of the NbO_6 octahedra is also significantly influenced by the lithium non-stoichiometry.

Finally, it must be emphasized that the stability of the other members of the series $Li_2A_{n-1}M_nO_{3n+1}$, should also be governed by the matching between the tetrahedral layers and the octahedral layers and that the size of the A site cation should also play a role since it influences the tilting of the octahedra. However we should bear in mind that the tilting is made more flexible as the thickness of the layer increases. In order to confirm this viewpoint, attempts were made to synthesize $n=3$ members with smaller A site cations than $Li_2Sr_{1.5}Nb_3O_{10}$.[10] The oxide $Li_2Ca_{1.5}Nb_3O_{10}$, the cell parameters of which are listed in Table 3, could be prepared as a single phase,whereas the $n=2$ member $Li_2CaNb_2O_7$ could not, which supports this hypothesis.

Table 3 Experimental lattice constants for lithium compounds

Compound	*x*	*a*/Å	*b*/Å	*c*/Å
$n=2$				
$Li_2Sr_{1-x}La_{2x/3}Nb_2O_7$	0.1	18.0409(6)	5.5969(2)	5.5907(3)
	0.2	18.0652(4)	5.5935(1)	5.5870(2)
	0.3	18.0708(4)	5.5898(2)	5.5837(2)
	0.4	18.0688(6)	5.5888(2)	5.5833(2)
	0.5	18.0772(6)	5.5867(3)	5.5818(3)
	0.6	18.0394(4)	5.5876(2)	5.5833(2)
	0.7	18.0229(4)	5.5861(2)	5.5819(2)
	0.8	18.0225(4)	5.5852(2)	5.5815(2)
	0.9	17.9927(8)	5.5819(4)	5.5782(5)
$Li_2Sr_{1-x}Nd_{2x/3}Nb_2O_7$	0.1	18.0354(6)	5.5935(2)	5.5864(2)
	0.2	18.0577(6)	5.5903(2)	5.5833(3)
	0.3	18.0372(8)	5.5911(3)	5.5834(3)
	0.4	18.0545(9)	5.5795(3)	5.5736(4)
	0.5	18.0853(9)	5.5718(5)	5.5681(5)
$Li_2Sr_{1-x}Eu_xTa_2O_7$	0.8	18.1870(11)	5.5850(4)	5.5783(4)
	1	18.1766(6)	5.5852(2)	5.5776(2)
$Li_2SrTa_2O_7$		18.189(1)	5.5919(6)	5.5768(4)
$Li_{1.8}Sr_{0.8}La_{0.2}Nb_2O_7$		18.213(1)	5.5822(8)	5.5794(8)
$Li_2SrNb_2O_7$		18.0071(5)	5.5979(3)	5.5920(3)
$n=3$				
$Li_2Ca_{1.5}Nb_3O_{10}$		26.221(1)	5.4874(3)	5.4874(3)

Concluding remarks

New $n=2$ members of the $Li_2A_{n-1}M_nO_{3n+1}$ family, involving tetrahedral Li_2O layers, have been synthesized for the first time using solid state reactions. The symmetry of these phases, belonging to the *Cmcm* space group, is different from that previously obtained for $LiAM_2O_7$ and $Li_2AM_2O_7$ members,[6–9] and implies alternate tilting of the [001] rows of octahedra in opposite directions, leading to a distorted tetrahedral coordination for lithium.

This study demonstrates the possibility of complex cationic non-stoichiometry, in both the tetrahedral layers and in the perovskite layers, according to the generic formula $Li_{2-y}A_{2-x}M_2O_7$. The crystal chemistry of these phases, and

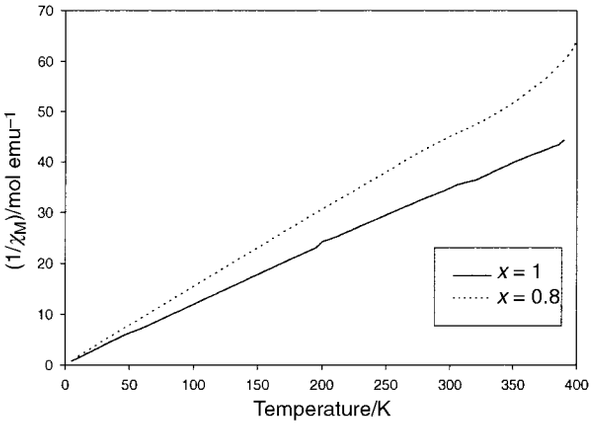

Fig. 6 Temperature dependance of χ_M^{-1} for $Li_2Sr_{0.2}Eu_{0.8}Ta_2O_7$ and $Li_2EuTa_2O_7$.

especially their stability, is governed by the matching between the octahedral and tetrahedral layers, so that the tilting of the octahedra within the perovskite layers probably plays a role in their stability. A systematic neutron diffraction study of different members of this series will be necessary to obtain a better understanding of this behavior.

NOTE: at the end of this work, we were informed of the study of Fourquet and coworkers[12] on $Li_2SrNb_2O_7$ (see preceding paper). Our results differ in terms of the choice of the space group for the structural determination.

Acknowledgements

We are grateful to Dr Françoise Bourée and M. Bernard Rieu for the collection of neutron diffraction data.

References

1 R. S. Ruddlesden and P. Popper, *Acta Crystallogr.*, 1957, **10**, 538.
2 M. Dion, M. Ganne and M. Tournoux, *Mater. Res. Bull.*, 1981, **16**, 1429.
3 M. Sato, J. Abo, T. Jin and M. Ohta, *J. Alloys Compd.*, 1993, **192**, 81.
4 M. Sato, J. Watanabe and K. Uematsu, *J. Solid State Chem.*, 1993, **107**, 460.
5 K. Hyeon and S. Byeon, *Chem. Mater.*, 1999, **11**, 352.
6 K. Toda and M. Sato, *J. Mater. Chem.*, 1996, **6**, 1067.
7 M. Sato, T. Jin and H. Ueda, *Chem. Lett.*, 1994, 161.
8 C. Bohnke, O. Bohnke and J. L. Fourquet, *J. Electrochem. Soc.*, 1997, **144**, 1151.
9 K. Toda, M. Takahashi, T. Teranishi, Z. Ye, M. Sato and Y. Hinatsu, *J. Mater. Chem.*, 1999, **9**, 799.
10 N. S. Bhuvanesh, M. P. Crosnier-Lopez, O. Bohnke, J. Emery and J. L. Fourquet, *Chem. Mater.*, 1999, **11**, 634.
11 J. Rodriguez-Carjaval, Abstracts of Satellite Meeting on Powder Diffraction of XVth Congr. Int. Union of Crystallography, Toulouse, 1990, p. 127.
12 N. S. P. Bhuvanesh, M. P. Crosnier-Lopez, H. Duroy and J. L. Fourquet, *J. Mater. Chem.*, 1999, **9**, 3093.

Paper 9/04416G